Response of the Southern Ocean overturning circulation to extreme Southern Annular Mode conditions

Kial Douglas Stewart[1], Andrew McC. Hogg[1], Matthew H. England[2], and Darryn W. Waugh[3]

[1]Australian National University
[2]University of New South Wales
[3]Johns Hopkins University

November 26, 2022

Abstract

The positive trend of the Southern Annular Mode (SAM) will impact the Southern Ocean's role in Earth's climate, however the details of the Southern Ocean's response remain uncertain. We introduce a methodology to examine the influence of SAM on the Southern Ocean, and apply this method to a global ocean–sea-ice model run at three resolutions (1$ˆ{\circ}$, 1/4$ˆ{\circ}$ and 1/10$ˆ{\circ}$). Our methodology drives perturbation simulations with realistic atmospheric forcing of extreme SAM conditions. The thermal response agrees with previous studies; positive SAM perturbations warm the upper ocean north of the windspeed maximum and cool it to the south, with the opposite response for negative SAM. The overturning circulation exhibits a rapid response that increases/decreases for positive/negative SAM perturbations and is insensitive to model resolution. The longer term adjustment of the overturning circulation, however, depends on the representation of eddies, and is faster at higher resolutions.

Posted on 26 Nov 2022 — CC-BY 4.0 — https://doi.org/10.1002/essoar.10503406.1 — This a preprint and has not been peer reviewed. Data may be preliminary.

Figure 1.

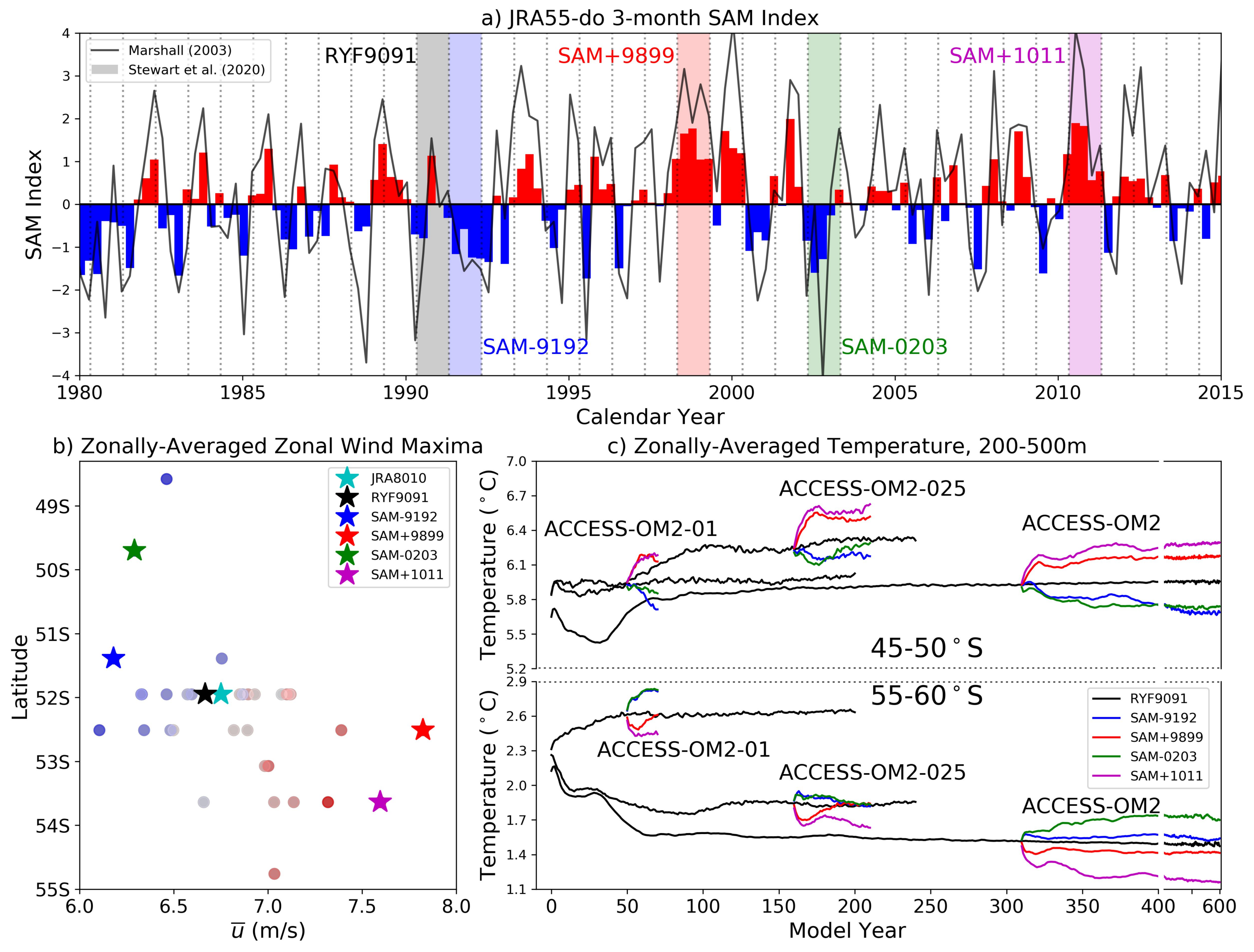

a) JRA55-do 3-month SAM Index
Marshall (2003)
Stewart et al. (2020)
RYF9091
SAM+9899
SAM+1011
SAM-9192
SAM-0203
SAM Index
Calendar Year
b) Zonally-Averaged Zonal Wind Maxima
JRA8010
RYF9091
SAM-9192
SAM+9899
SAM-0203
SAM+1011
Latitude
$\overline{u}$ (m/s)
c) Zonally-Averaged Temperature, 200-500m
ACCESS-OM2-025
ACCESS-OM2-01
ACCESS-OM2
45-50°S
55-60°S
Temperature ($^\circ$C)
Model Year

Figure 2.

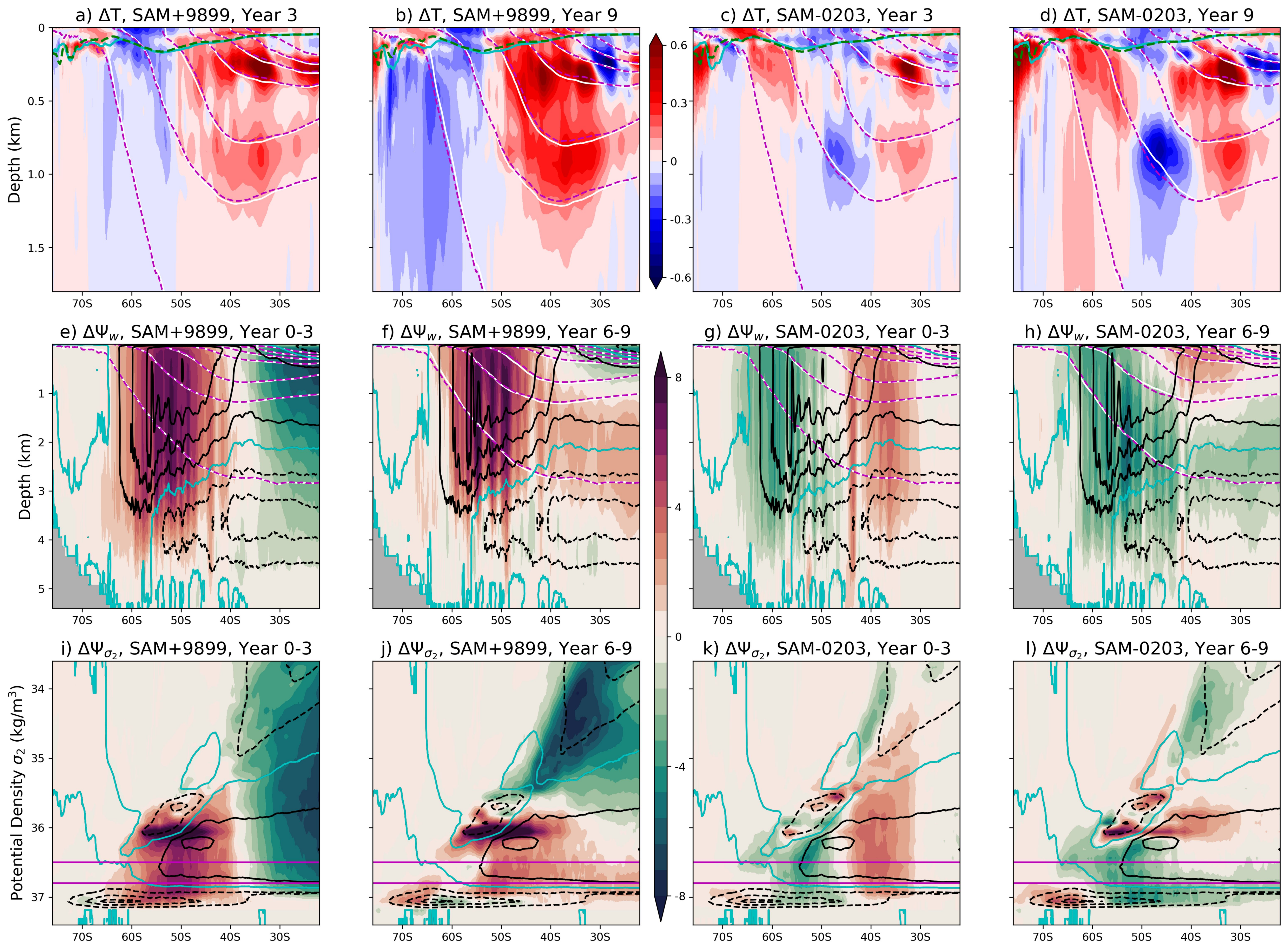
a) ΔT, SAM+9899, Year 3
b) ΔT, SAM+9899, Year 9
c) ΔT, SAM-0203, Year 3
d) ΔT, SAM-0203, Year 9
e) $\Delta\Psi_w$, SAM+9899, Year 0-3
f) $\Delta\Psi_w$, SAM+9899, Year 6-9
g) $\Delta\Psi_w$, SAM-0203, Year 0-3
h) $\Delta\Psi_w$, SAM-0203, Year 6-9
i) $\Delta\Psi_{\sigma_2}$, SAM+9899, Year 0-3
j) $\Delta\Psi_{\sigma_2}$, SAM+9899, Year 6-9
k) $\Delta\Psi_{\sigma_2}$, SAM-0203, Year 0-3
l) $\Delta\Psi_{\sigma_2}$, SAM-0203, Year 6-9
Depth (km)
Potential Density σ_2 (kg/m^3)
70S 60S 50S 40S 30S
0.6 0.3 0 -0.3 -0.6
8 4 0 -4 -8

Figure 3.

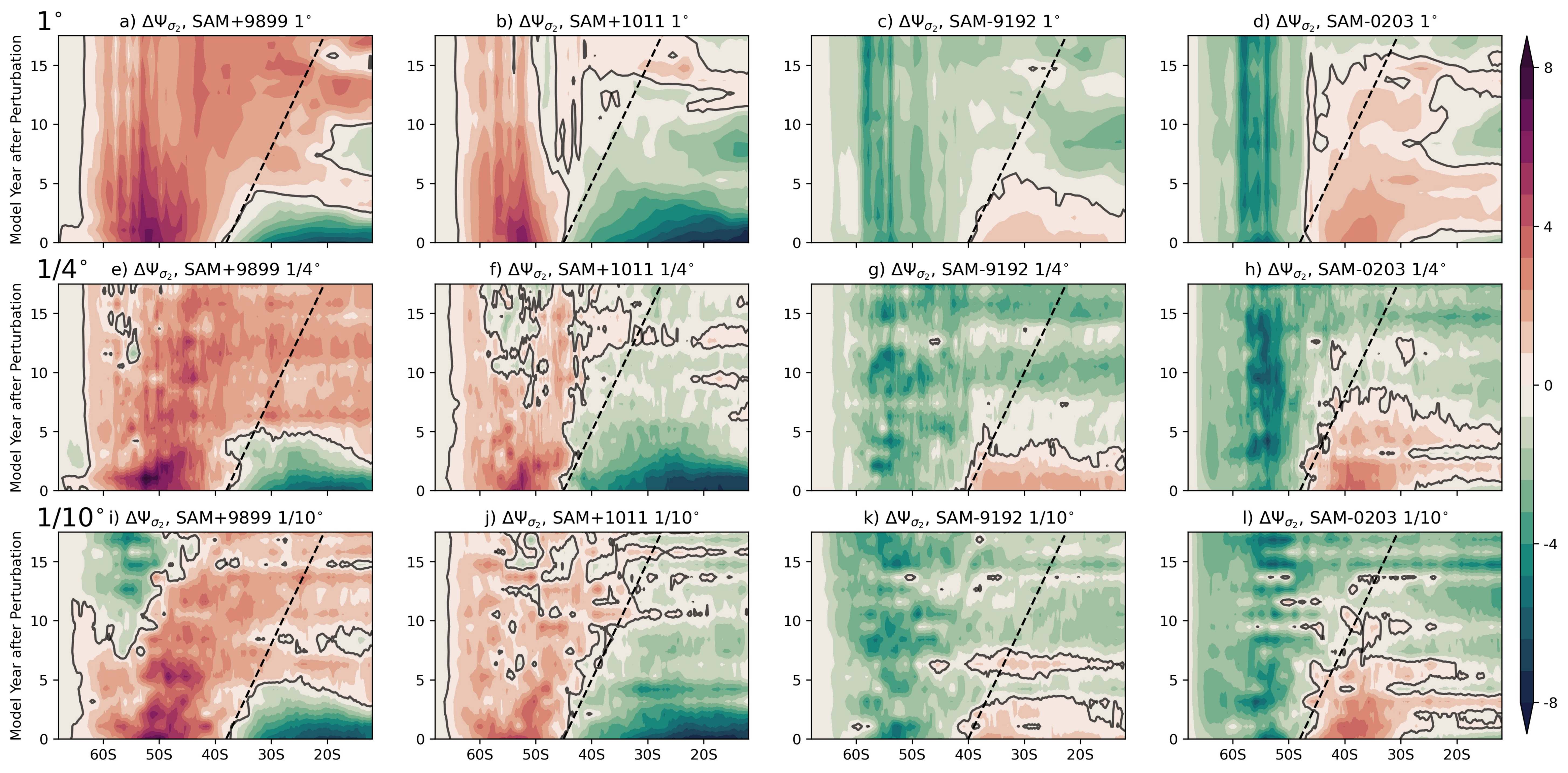

1°
a) $\Delta\Psi_{\sigma_2}$, SAM+9899 1°
b) $\Delta\Psi_{\sigma_2}$, SAM+1011 1°
c) $\Delta\Psi_{\sigma_2}$, SAM-9192 1°
d) $\Delta\Psi_{\sigma_2}$, SAM-0203 1°
1/4°
e) $\Delta\Psi_{\sigma_2}$, SAM+9899 1/4°
f) $\Delta\Psi_{\sigma_2}$, SAM+1011 1/4°
g) $\Delta\Psi_{\sigma_2}$, SAM-9192 1/4°
h) $\Delta\Psi_{\sigma_2}$, SAM-0203 1/4°
1/10°
i) $\Delta\Psi_{\sigma_2}$, SAM+9899 1/10°
j) $\Delta\Psi_{\sigma_2}$, SAM+1011 1/10°
k) $\Delta\Psi_{\sigma_2}$, SAM-9192 1/10°
l) $\Delta\Psi_{\sigma_2}$, SAM-0203 1/10°
Model Year after Perturbation
0
5
10
15
60S
50S
40S
30S
20S
8
4
0
-4
-8

Figure 4.

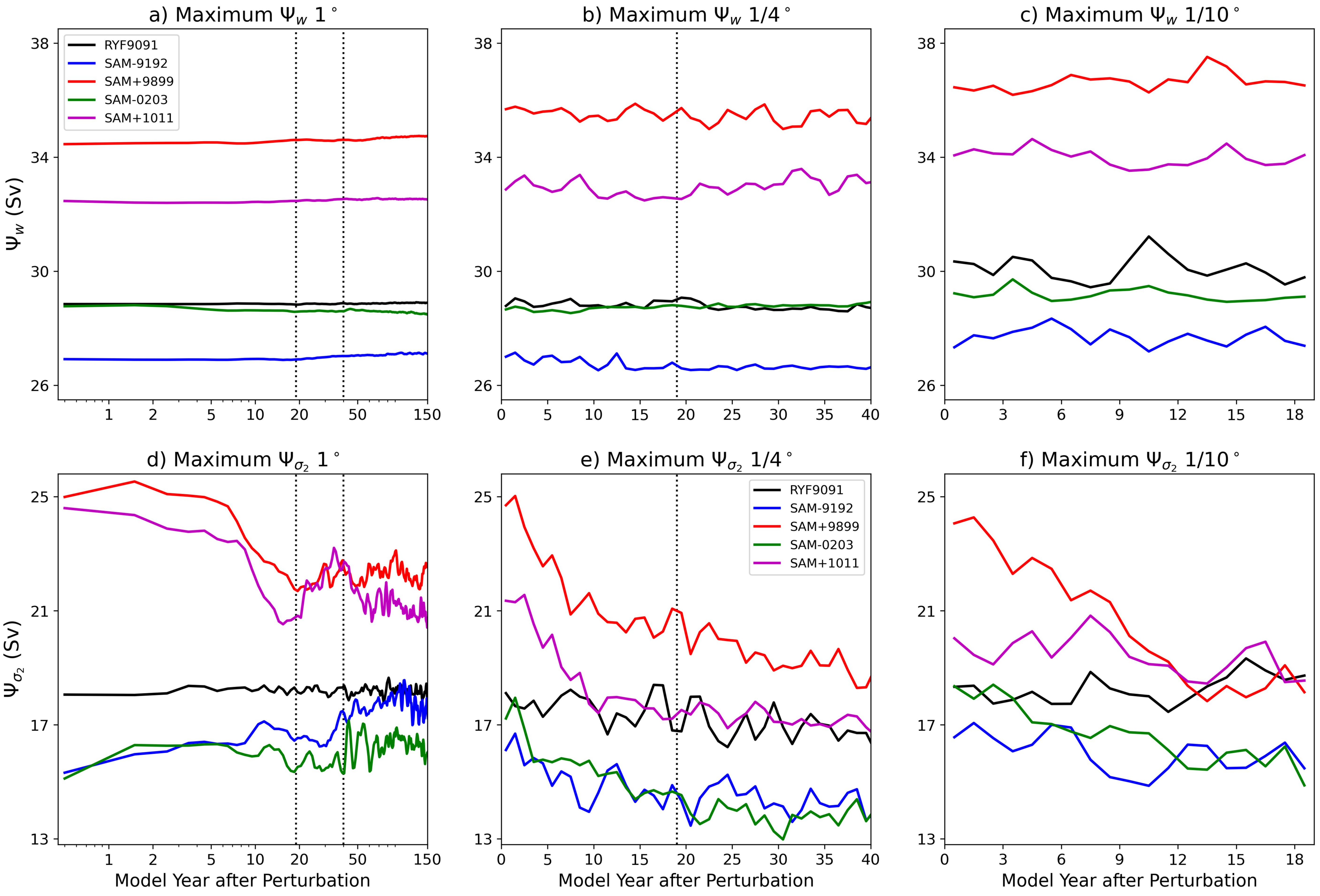

a) Maximum Ψ_w 1°
b) Maximum Ψ_w 1/4°
c) Maximum Ψ_w 1/10°
d) Maximum Ψ_{σ_2} 1°
e) Maximum Ψ_{σ_2} 1/4°
f) Maximum Ψ_{σ_2} 1/10°
Ψ_w (Sv)
Ψ_{σ_2} (Sv)
RYF9091
SAM-9192
SAM+9899
SAM-0203
SAM+1011
Model Year after Perturbation

Response of the Southern Ocean overturning circulation to extreme Southern Annular Mode conditions

K.D. Stewart[1,2], A.McC. Hogg[1,3], M.H. England[2,3], and D.W. Waugh[4,5]

[1]Research School of Earth Sciences, Australian National University, Canberra, Australia
[2]Climate Change Research Centre, University of New South Wales, Sydney, Australia
[3]Australian Research Council Centre of Excellence for Climate Extremes
[4]Department of Earth and Planetary Sciences, The Johns Hopkins University, Baltimore, USA
[5]School of Mathematics and Statistics, University of New South Wales, Sydney, Australia

Key Points:

- New methodology to examine the Southern Ocean response to climate extremes using perturbation simulations with realistic atmospheric forcing
- Southern Ocean overturning circulation exhibits a rapid response that is sustained in depth-latitude space, but decays in density-latitude space
- Adjustment of the ocean interior occurs along isopycnals at a rate of order 1° latitude per year, depending of the representation of eddies

Corresponding author: K.D. Stewart, `kial.stewart@anu.edu.au`

Abstract

The positive trend of the Southern Annular Mode (SAM) will impact the Southern Ocean's role in Earth's climate, however the details of the Southern Ocean's response remain uncertain. We introduce a methodology to examine the influence of SAM on the Southern Ocean, and apply this method to a global ocean–sea-ice model run at three resolutions (1°, 1/4° and 1/10°). Our methodology drives perturbation simulations with realistic atmospheric forcing of extreme SAM conditions. The thermal response agrees with previous studies; positive SAM perturbations warm the upper ocean north of the windspeed maximum and cool it to the south, with the opposite response for negative SAM. The overturning circulation exhibits a rapid response that increases/decreases for positive/negative SAM perturbations and is insensitive to model resolution. The longer term adjustment of the overturning circulation, however, depends on the representation of eddies, and is faster at higher resolutions.

Plain Language Summary

The Southern Ocean has accounted for the vast majority of the global ocean heat uptake since the early 2000s. The atmospheric winds over the Southern Ocean play a leading role in its ability to uptake heat, by way of driving much of the Southern Ocean circulation. Observations of these winds indicate that they have been steadily changing over the past few decades, and hence, so too is the Southern Ocean heat uptake. However, despite recent research efforts, the details of the Southern Ocean's response to these changing winds remain uncertain. Here we introduce a novel methodology to examine the Southern Ocean's response to changing winds. We perform numerical simulations with a global ocean–sea-ice model suite that spans a hierarchy of spatial resolutions and driven by realistic atmospheric forcing conditions. The initial response of the Southern Ocean circulation to changes in winds is robust across the model suite and insensitive to model resolution; longer-term response, however, depends on the representation of eddies in the model.

1 Introduction

The Southern Ocean has accounted for between 67%–98% of the total ocean heat uptake since 2005 (Roemmich et al., 2015; Llovel & Terray, 2016). This Southern Ocean heat uptake, which is predominantly in the upper 2 km, results from the intricate interplay between surface fluxes of heat and momentum, ocean circulation, and the associated redistribution of existing oceanic heat reservoirs (Frölicher et al., 2015; J. Marshall et al., 2015; Armour et al., 2016). Southern Hemisphere winds play a leading role in these proposed mechanisms of Southern Ocean heat uptake. It follows that Southern Ocean heat uptake, and thus global ocean warming, will be sensitive to processes that govern Southern Hemisphere winds.

The Southern Annular Mode (SAM) is the primary mode of climate variability in the extratropical Southern Hemisphere (Thompson & Wallace, 2000; Thompson et al., 2000). The SAM dynamically influences the strength and latitudinal location of the Southern Hemisphere midlatitude westerly winds. Following Gong and Wang (1999), the SAM can be characterised by a SAM index based on the normalized monthly zonal mean sea level pressure difference between 40°S and 65°S. Observations indicate there has been a positive trend in the SAM index since the 1950s (Thompson & Solomon, 2002; G. Marshall, 2003), which is projected to continue due to anthropogenic forcing (Zheng et al., 2013). It is anticipated that this trend in the SAM index, and the associated trends in the strength and position of the Southern Hemisphere midlatitude westerly winds, will influence Southern Ocean warming (e.g., Armour et al., 2016).

Examining the influence of the SAM on the Southern Ocean often employs regression and/or correlation analysis techniques, instantaneous or time-lagged, to ascribe changes in the ocean state with the value of the SAM index. This approach is particularly useful for studies that use satellite- or Argo-based observations, coupled climate model output, or reanalysis products (e.g. Lovenduski & Gruber, 2005; Kosempa & Chambers, 2014; Sen Gupta & England, 2006; Hazel & Stewart, 2019). Another approach is to examine composites of ocean states based on SAM index thresholds to average out signals that are not SAM-related (e.g., Sallèe et al., 2010; Li et al., 2019). Such methodologies are convenient since the independent variable (the SAM index) is unable to be controlled in these datasets; however, the transient response of the system may act to obscure correlations. These approaches demonstrate that of all the atmospheric variability associated with the SAM, the Southern Ocean is most sensitive to the SAM-related changes in wind forcing (e.g., Sen Gupta & England, 2006).

An alternative approach to understand the influence of SAM in the Southern Ocean uses perturbation simulations. Given that the Southern Ocean is most sensitive to the wind changes associated with SAM, these simulations typically consist of an extended duration control run driven by repeating year forcing, from which perturbation runs are branched. These perturbation simulations have some idealised modification of their wind forcing fields stylised on the SAM associated strengthening and/or poleward shifting of the Southern Hemisphere midlatitude westerly winds (e.g., Farneti et al., 2010; Gent & Danabasoglu, 2011; Hofmann & Morales-Maqueda, 2011; Spence et al., 2014; Waugh et al., 2019). Note that the focus of these SAM-influenced perturbation studies has been to understand the response of the Southern Ocean to the observed positive trend in the SAM, and as such they generally do not impose forcing anomalies representative of negative SAM conditions. Nevertheless, this approach has the advantage, and disadvantage, that the idealised wind anomalies can be manipulated in time, space, structure and magnitude, such that the permutations of the anomaly configuration are without limit. Given the multitude of anomaly permutations, a sensible approach is to keep the anomaly configuration as simple as possible, which begs the question: is the Southern Ocean response fundamentally different if *any* complexity is added to the anomaly? Another important consideration for such experiments is that the idealised wind anomalies are typically applied without regard to other aspects of the climate that then become physically inconsistent. For instance, a real poleward shifting of the wind field would be accompanied by a shift of the storm tracks, as well as the cloud cover and air temperatures; these forcing fields typically remain unmodified in the perturbation simulations.

Here we introduce a new methodology to simulate and examine the influence of SAM on the Southern Ocean in a global ocean–sea-ice model that uses realistic, reanalysis-based, repeating year atmospheric forcing to drive both control and SAM perturbation simulations. For the control forcing, the repeating year is a period of climatologically-neutral conditions; for the perturbations, the repeating years are periods of both extreme positive and extreme negative SAM conditions. While this approach brings an increased level of complexity to the dynamical structure of the perturbation, it greatly reduces the subjectivity of the perturbation configuration, and maintains the physical consistency of its forcing fields. This methodology is described in §2, and the thermal response of the Southern Ocean to the extreme SAM forcing conditions is presented in §3. We then compare the response of the Southern Ocean overturning circulation to the extreme SAM forcing conditions, examining the overturning in both depth-latitude and density-latitude coordinates (§4). Finally §5 covers the summary of our results and conclusions.

2 Model & Methodology

We employ the Australian Community Climate and Earth System Simulator, ocean–sea-ice model version 2 (ACCESS-OM2; Kiss et al., 2020), a modelling suite developed by the Consortium for Ocean–Sea-Ice Modelling in Australia (COSIMA), to simulate the global ocean–sea-ice response to changes in imposed atmospheric conditions. This suite includes global ocean–sea-ice model configurations with horizontal grid spacings of nominally 1° (ACCESS-OM2), 0.25° (ACCESS-OM2-025) and 0.1° (ACCESS-OM2-01) latitude and longitude; here we use all three configurations. Following Stewart et al. (2017), the grid spacings of the generalized z* vertical coordinate of the ocean models are objectively-constructed to support the vertical structure of the baroclinic dynamics permitted by the horizontal grids. The two coarser configurations implement the Gent and McWilliams (1990) (GM) parameterisation to represent under-resolved mesoscale eddies with an associated diffusivity that is flow-dependent (see Griffies et al., 2005) and scaled by the ability of the horizontal grid to resolve the first baroclinic Rossby radius (as per Hallberg, 2013), and the Redi (1982) parameterisation for along-isopycnal diffusion with a coefficient of $600\,\mathrm{m}^2/\mathrm{s}$ for ACCESS-OM2 and up to $200\,\mathrm{m}^2/\mathrm{s}$ for ACCESS-OM2-025 (scaled by the local grid resolution and Rossby radius). For further details and evaluation of the ACCESS-OM2 suite see Kiss et al. (2020).

The ACCESS-OM2 simulations are initialised with January temperature and salinity fields from the World Ocean Atlas 2013 (WOA13; Locarnini et al., 2013; Zweng et al., 2013). The simulations are forced with prescribed atmospheric conditions taken from the high-resolution, self-consistent Japanese atmospheric reanalysis dataset for driving ocean models (JRA55-do; Tsujino et al., 2018). These prescribed atmospheric conditions, described in detail by Stewart et al. (2020), are the 12-month period from 1st May 1990 to 30th April 1991 used repeatedly to drive the simulations. In practice, the forcing runs from 1st January 1991 to 31st December 1990 with a sudden transition from 30th April 1991 back to 1st May 1990; shifting the sudden transition away from the December solstice reduces the intensity of weather variability at the time of transition. This repeated year forcing period, referred to as RYF9091, has been identified as a quasi-climatological period of the JRA55-do dataset with neutral values of all major climate indices, including the SAM index (see Fig. 1a). These RYF9091 simulations have two primary purposes; they provide for an extended period of model adjustment from the WOA13 state over which the model drift can be assessed, and they serve as control simulations from which perturbation simulations can be branched and compared.

A further four forcing periods are identified from the JRA55-do record; these are 12-month periods, running 1st May to 30th April of the following year, with anomalous (positive and negative) Southern Annular Mode conditions, collectively referred to as SAMx periods. The extreme negative SAMx periods (SAM- years) are 1991–1992 and 2002–2003, and the extreme positive SAMx periods (SAM+ years) are 1998–1999 and 2010–2011 (Fig. 1a); these periods are referred to as SAM-9192, SAM-0203, SAM+9899 and SAM+1011, respectively, and are used to drive perturbation simulations branched from the RYF9091 control simulations. The annual averages of the zonally-averaged zonal winds of the SAMx periods are shown in Figure 1b; the relationship between the SAM index and the wind speed strength and latitudinal distribution is evident, as well as the degree to which our identified SAMx periods are extreme. For reference, the relative differences in the zonally-averaged zonal winds between the SAMx and RYF9091 periods are distinct for the SAM+ and SAM- cases, and reach +30% for the SAM+ and -15% for the SAM- periods. While these large changes in the wind fields dominate the atmospheric signature of extreme SAM periods, our technique has the advantage that synchronous changes in other fields (including the buoyancy forcing) are naturally included. Additionally, the respective increase or decrease of the wind speed maxima for a given SAMx forcing period is mirrored northwards of ∼45°S, such that, for instance, the zonal wind speed of the SAM+ periods is less than the JRA55-do climatological mean; this is a forcing feature that is typically not included in experiments with idealised wind perturbations (e.g., Spence et al., 2014).

The RYF9091 control simulations are initialised from rest with the WOA13 hydrography and run for 600, 240 and 200 years for the 1°, 0.25° and 0.1° model configurations,

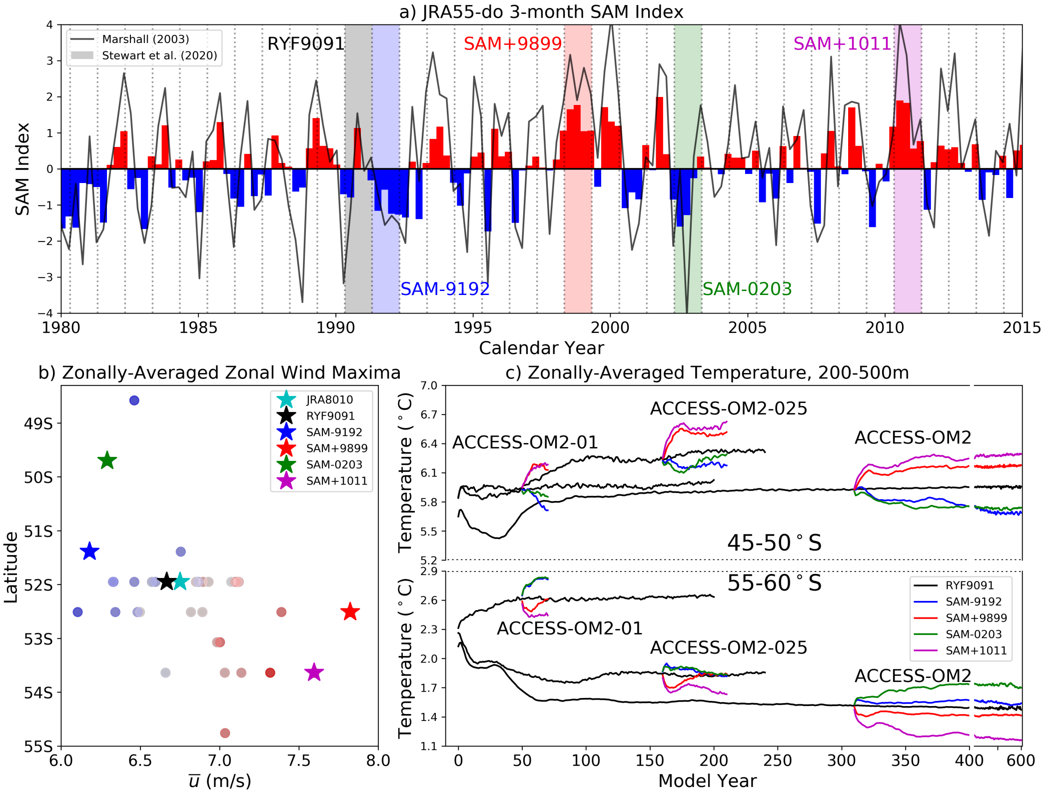

Figure 1. a) Three-monthly SAM index calculated from the JRA55-do dataset. The RYF9091 and four SAMx periods are shaded. For comparison, the equivalent observational station-based SAM index of G. Marshall (2003) is included in black. b) The zonally-averaged zonal wind maximum speed and latitudinal locations for the RYF9091 and SAMx periods. Also included is the 1980–2010 average of the JRA55-do dataset (JRA8010; cyan star) as a climatological reference, and all remaining May–April periods between 1980–2015 coloured blue–red by their respective SAM index (dots). c) Timeseries of the simulated zonally-averaged temperatures between 200–500m depth for 45–50°S (upper) and 55–60°S (lower); these latitudinal bands are selected to lie either side of the zonal wind speed maxima.

respectively. Following an initial adjustment period (310, 160 and 50 years for the 1°, 0.25° and 0.1° model configurations, respectively; Fig. 1c), simulations with the SAMx forcing conditions are branched off and run alongside the control simulations for 290, 50 and 20 years for the 1°, 0.25° and 0.1° model configurations, respectively. This methodology allows for the direct comparison of the perturbation–control differences across the suite of model configurations. Whilst the primary focus of the analysis here is the response of the Southern Ocean overturning circulation, to begin with we briefly examine the zonally-averaged thermal responses.

3 Thermal Response

The initial response of the upper Southern Ocean temperature to the sudden change in forcing is consistent with previous studies (e.g., Gent & Danabasoglu, 2011); north of the zonal wind speed maximum the upper ocean temperatures increase for SAM+ perturbations (and decreases for SAM- perturbations) by approximately 0.2°C within 5 years, with the opposite response occurring south of the zonal wind speed maximum (Fig. 1c). The magnitude and timescale of these initial responses are distinct from the gradual temperature changes arising from model drift, and insensitive to model resolution. Following an initial adjustment period, these thermal responses are either sustained for the duration of the perturbation simulations, or trend back towards the respective RYF9091 simulation; importantly, they do not continue to grow with time.

Figure 2(a-d) depicts the depth-latitude distributions of the zonally-averaged temperature anomalies for the (a,b) SAM+9899 and (c,d) SAM-0203 forced ACCESS-OM2-01 simulations, averaged for the (a,c) third and (b,d) ninth years after the perturbation. The SAM+9899 perturbation exhibits thermal anomaly distributions that are consistent with the south–north cooling–warming response straddling the wind speed maximum previously described by Sen Gupta and England (2006). The thermal response of the SAM-0203 perturbation exhibits relatively more structure, but of reduced intensity compared to the SAM+9899 response. Equivalent temperature anomaly distributions for the SAM+1011 and SAM-9192 simulations are presented in Figure S1; the comparison of these figures highlights the consistent thermal response of the respective SAM+ and SAM- cases, particularly south of 30°S for SAM+ and 40°S for SAM-. All cases exhibit local extrema in the thermal responses at around 800–900 m depth; for SAM+ this occurs between 35–45°S, and for SAM- between 40–50°S. Comparing the thermal anomaly distributions for the Year 3 and Year 9 responses shows that, whilst the thermal responses intensify in time, they retain their initial structure.

The zonally-averaged temperature anomalies are comprised of a combination of processes which include the wind-driven movement of isopycnals, defined as "heave" by Bindoff and McDougall (1994), and the change of temperature on isopycnals due to changes of along isopycnal transport and stirring. In the figures of zonally-averaged temperature anomaly, heave is evidenced by the spatial correlation between the vertical displacement of isopycnals and the sign of the thermal anomalies. The diagnosed contributions from heave and the change of temperature on isopycnals for the SAM+9899 and SAM-0203 cases at all three model resolutions are shown in Figure S2. The contribution from heave is insensitive to model resolution, which is perhaps to be expected as to leading order heave is a wind-driven process. Heave is strongest north of 50°S and accounts for the local extrema in the thermal responses around 800–900 m depth. The contribution from temperature changes on isopycnals, however, is surface intensified, strongest south of 50°S, and resolution-dependent; this distribution makes sense considering the important role that eddies play in along isopycnal stirring and transport. Timeseries of these contributions to the thermal anomalies north and south of the wind speed maxima show the longer-term thermal responses (Fig. S3); importantly, the SAM+ and SAM- perturbations are distinct in all cases. South of the wind speed maxima, the change of temperature on isopycnals dominates over the heave-associated response and strengthens with refined model resolution. North of the wind speed maxima, however, the heave and isopycnal temperature changes have contributions of similar magnitude and appears insensitive to model resolution.

4 Overturning Circulation Response

Considering the rapid timescale of thermal adjustment, the initial dominance of heave, and the structure of the thermal anomalies relative to the wind speed maxima, the thermal response indicates a wind-driven modification of the Southern Ocean overturning circulation. To examine the response of the overturning circulation, we evaluate and compare two overturning streamfunctions independently diagnosed from the simulations. Following Zika et al. (2012), the first streamfunction Ψ_w (m^2/s) is derived by integrating the vertical velocity in longitude and northward from the Antarctic coastline up a given latitude y, that is,

$$\Psi_w(y,z,t) = \int_{90^\circ S}^{y} \int w(x,y',z,t)\, dx dy', \tag{1}$$

where w is the annually-averaged vertical velocity, giving Ψ_w in depth-latitude-time coordinates. Taking σ_2 as the potential density of seawater referenced to 2000 dbar less 1000 kg/m^3, a second overturning streamfunction Ψ_{σ_2} (m^2/s) can be diagnosed by integrating the along-isopycnal meridional velocity in longitude and from the densest isopycnal class ($\sigma_2 >$ 38) to a given isopycnal σ_2, as,

$$\Psi_{\sigma_2}(y,\sigma_2,t) = \int_{38}^{\sigma_2} \int v_{\sigma_2}(x,y,\sigma_2',t)\, dx d\sigma_2', \tag{2}$$

where v_{σ_2} is the along-isopycnal meridional velocity, returning Ψ_{σ_2} in density-latitude-time coordinates. We refer to these two overturning streamfunctions as the w-streamfunction and σ_2-streamfunction, respectively.

The depth-latitude distributions of $\Delta\Psi_w$ for the ACCESS-OM2-01 cases of SAM+9899 and SAM-0203 are shown in Figure 2e-h; these are 3-year averages for the Years 0–3 (e,g) and 6–9 (f,h). The initial responses of $\Delta\Psi_w$ are seemingly depth-independent above ∼3000 m. In time, the w-streamfunction anomalies equatorward of 40-45°S develops vertical structure that appears to propagate along isopycnals; note that the Ψ_w anomalies poleward of 40-45°S maintain their initial structure and intensity. For the SAM+ cases, the structure, magnitude and evolution of the Ψ_w response is similar to that of the high-resolution simulations reported in previous studies (e.g., Farneti & Delworth, 2010), however we do not find the Ψ_w response to be resolution dependent. Given the implementation of a variable, flow-dependent GM diffusivity in the ACCESS-OM2 simulations at coarser resolutions, this insensitivity of the Southern Ocean response to the model resolution is indeed to be expected (Gent, 2016).

The interior structure of the time-evolution of these overturning circulation responses is more apparent in the σ_2-streamfunction anomalies (Fig. 2i-l). The Year 0-3 $\Delta\Psi_{\sigma_2}$ anomalies depend primarily on latitude for densities greater than ∼35.5kg/m^3. By Year 6-9 these anomalies have become more dependent on density and less dependent on latitude. The structure of the longer-term distributions of $\Delta\Psi_{\sigma_2}$, especially south of 40°S, tends to align with isopycnals and appears to propagate northwards.

The progression of the Ψ_{σ_2} anomalies into the interior along isopycnal pathways can be seen in time-latitude Hovmöller diagrams, for which we use the mean of the σ_2 range 36.5–36.8kg/m^3 (Fig. 3). The initial responses of all perturbations are insensitive to the model resolutions used here, and are characterised by regions of opposite signed signals either side of ∼40-45°S. In time, the equatorward signal diminishes, and in the cases of SAM+9899 and SAM-9192, vanishes within 5-8 years. For the SAM+ simulations with ACCESS-OM2-01, the boundary separating the opposite signed signals is observed to propagate equatorward at a rate of order 1° of latitude per year (dashed black lines in Fig. 3). For reference, this rate of propagation corresponds to an along-isopycnal diffusion with a coefficient of 390 m^2/s. The latitudinal progression of this signal represents the adiabatic, along-isopycnal propagation of a wind-forcing perturbation into the ocean interior (e.g., Doddridge et al., 2016). That is, the perturbation of the wind field initially excites an Eulerian response that is largely barotropic in nature and with the same latitudinal structure as the wind perturbation (Fig. 2e,g); in time, this initial Eulerian response penetrates equatorward into the ocean interior, predominantly adiabatically along isopycnals, a process that is likely dependent on eddies (parameterised or resolved), and hence model resolution. This demonstration of the initial and time-evolving adjustments reflects the multiple timescale responses that can arise from a changes in atmospheric forcing over the Southern Ocean (e.g., Armour et al., 2016; Waugh & Haine, 2020).

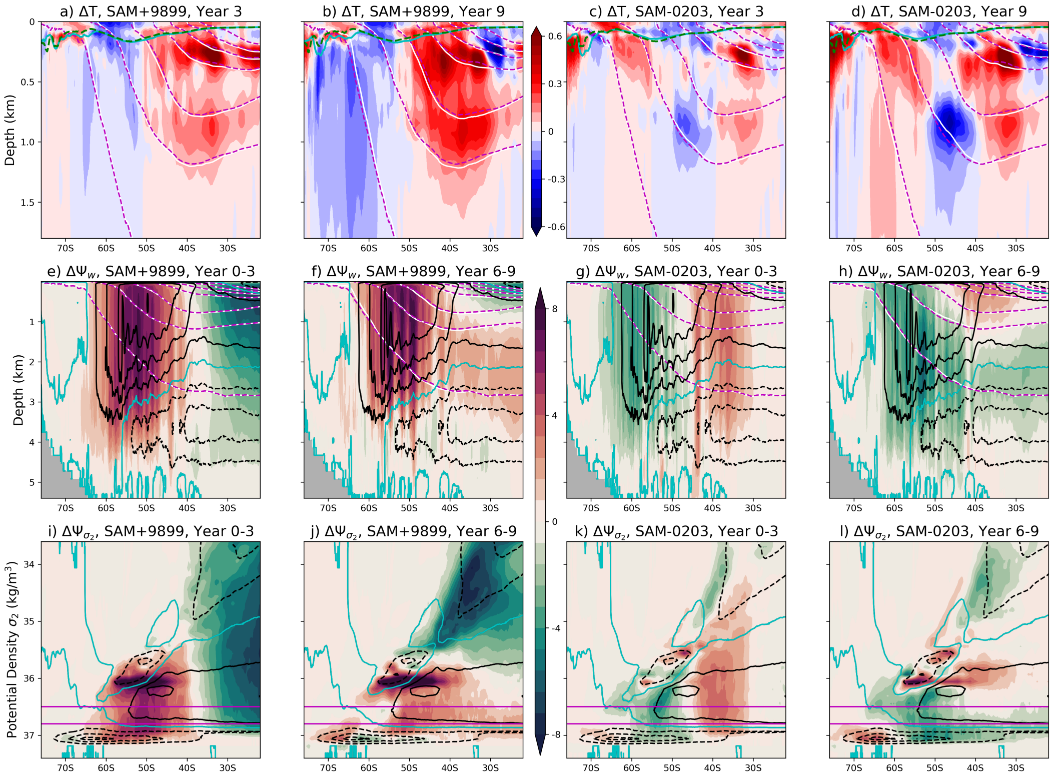

Figure 2. a-d) Distributions of the Year 3 (a,c) & 9 (b,d) temperature anomalies from the 0.1° ACCESS-OM2-01 for (a,b) SAM+9899 and (c,d) SAM-0203 simulations. The white and dashed magenta contours represent the SAMx and RYF9091 isopycnals at $\sigma_2 = 0.5\,\mathrm{kg/m^3}$ intervals, respectively, spanning $\sigma_2 = 34$–$37\,\mathrm{kg/m^3}$ inclusive, with the cyan and dashed green contours representing the respective mixed-layer depths. e-h) The w-streamfunction anomalies of the ACCESS-OM2-01 simulations with SAM+9899 (e,f) and SAM-0203 (g,h) averaged for the years 0-3 (e,g) and 6-9 (f,h). Contoured in black is the Ψ_w for the RYF9091 case at $\pm 7.5\,\mathrm{Sv}$ intervals with the $0\,\mathrm{Sv}$ contour in cyan. The white and dashed magenta contours represent the same isopycnals as in (a-d). Panels (i-l) depict a similar analysis to panels (e-h) but for the σ_2-streamfunction anomalies. The magenta lines in (i-l) at 36.5 and $36.8\,\mathrm{kg/m^3}$ indicate the regions of interest for Figure 3.

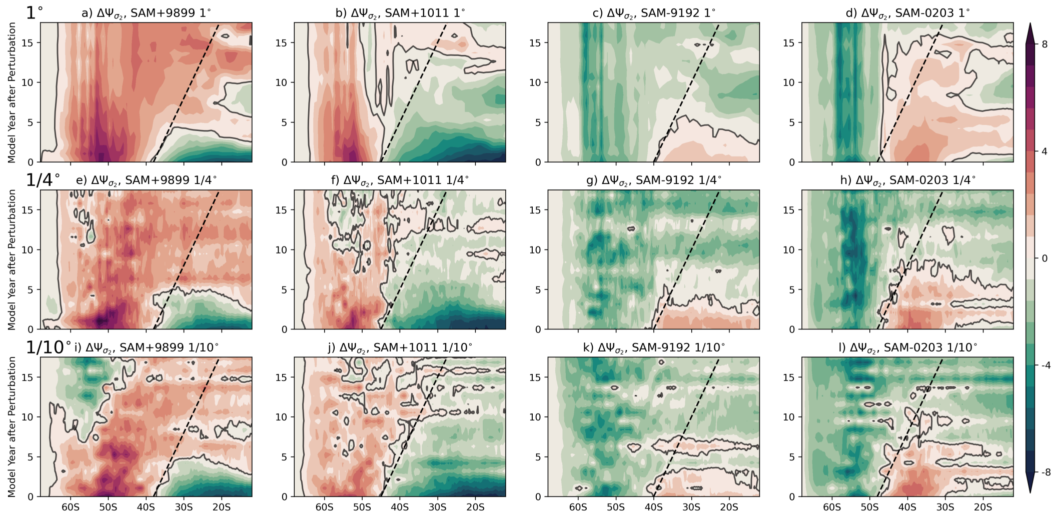

Figure 3. Hovmöller diagrams of the σ_2-streamfunction anomalies for the SAM+9899, SAM+1011, SAM-9192 and SAM-0203 cases (columns 1-4, respectively) and the 1°, 1/4° and 1/10° simulations (rows top-to-bottom, respectively). The $\Delta\Psi_{\sigma_2}$ is calculated as the 36.5–36.8kg/m^3 average, as indicated in Figure 2i-l. The $\Delta\Psi_{\sigma_2} = 0\,$Sv contour is included for reference, as well as the dashed slope which represents an along-isopycnal velocity of 1° latitude per year.

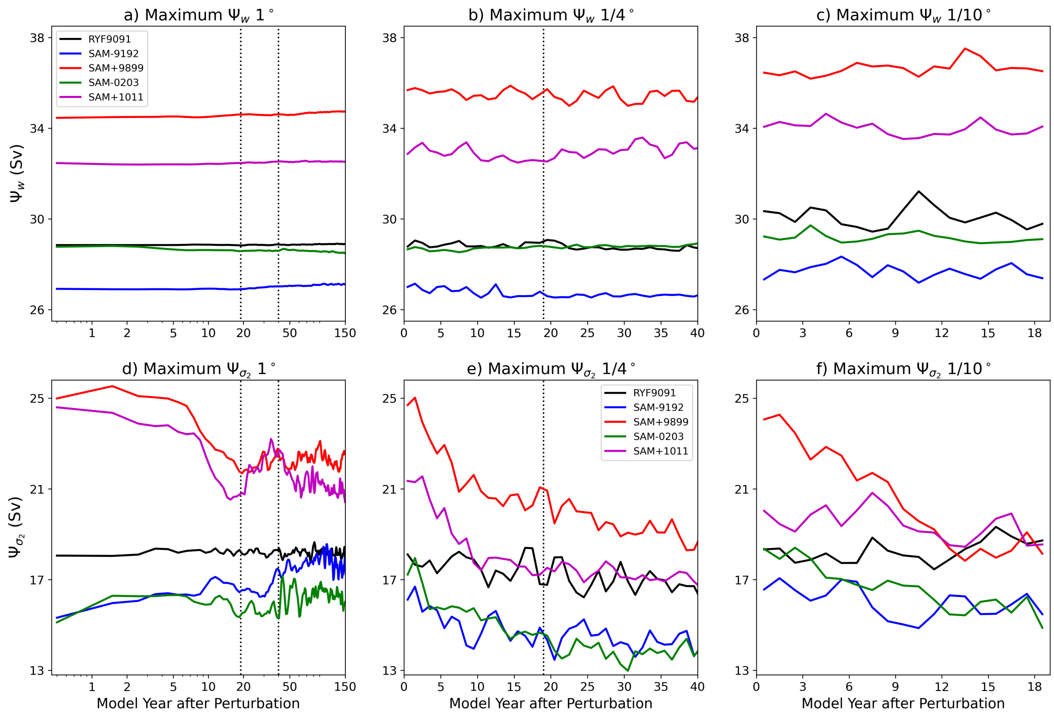

Figure 4. Timeseries of the maximum 24-month mean Ψ_w (a-c), Ψ_{σ_2} (d-f). Note the different time axes for different resolutions (columns); the vertical dotted lines in the ACCESS-OM2 and ACCESS-OM2-025 plots indicate the extent of the timeseries of the higher resolution panels.

An additional measure of the Southern Ocean overturning circulation response can be found by comparing the 24-month mean maxima of Ψ_w and Ψ_{σ_2} for the region of interest (south of 30°S). In the case of Ψ_w, the Southern Ocean maximum represents the strength of the "Deacon cell", a localised wind-driven overturning of waters in Eulerian space with near-uniform properties such that it is unable to substantially contribute to the meridional transport of tracer (e.g., Zika et al., 2012). Figure 4a-c shows the Southern Ocean maximum of Ψ_w increases for SAM+ and decreases for SAM- perturbations, and that this response does not evolve in time. This immediate and sustained response of the Ψ_w overturning streamfunction is consistent with the findings of Treguier et al. (2010), who report a high correlation ($r = 0.79$) between the Southern Ocean mean flow overturning and the SAM index in a global ocean–sea-ice simulation driven by atmospheric forcing with interannual variability.

The Southern Ocean maximum of Ψ_{σ_2} (Fig. 4d-f), however, initially exhibits a response that is of similar magnitude to the respective Ψ_w response, but is time dependent. The magnitude of the initial Ψ_{σ_2} maxima anomaly decreases as the model resolution is refined (compare the initial differences between the Ψ_{σ_2} maxima of SAMx and RYF9091 across the resolutions). For the SAM+ cases, the Ψ_{σ_2} maxima decays back towards the RYF9091 value with an adjustment timescale of approximately a decade for the 0.1° resolution case, and longer for the coarser resolutions. The Ψ_{σ_2} maxima of the SAM- cases are initially less than that of the RYF9091 and appear to continue decreasing for the first two decades; the longer, coarser resolution simulations suggest these Ψ_{σ_2} values stabilise for a couple of decades before returning towards the RYF9091 level. The initial response of the Ψ_{σ_2} is consistent with the results of Farneti et al. (2015), who found the correlation between the Southern Ocean upper cell overturning in density space and the SAM index of a multi-model ensemble to be high ($r = 0.67$), but not as high as that of Treguier et al. (2010) for the mean flow overturning. Farneti et al. (2015) also report that the Ψ_{σ_2}-SAM correlations of their various models are weaker for models with more responsive eddy fluxes ($r = 0.56$), and stronger for models with less responsive eddy fluxes ($r = 0.82$). In the context of our findings of the time-dependent Ψ_{σ_2} response, a stronger rate of decay, indicative of a weakening of the Ψ_{σ_2}-SAM correlation, can be interpreted as more responsive eddy fluxes, with the timescale of adjustment being set by the spin-up time of the eddy field. This interpretation is consistent with the increased initial Ψ_{σ_2} response for the coarser resolution simulations.

The results presented here demonstrate that the response of the Southern Ocean overturning circulation to sudden and extreme perturbations of SAM conditions is comprised of;

- a rapid and sustained adjustment of the wind-driven Deacon cell, represented here as Ψ_w, that increases for SAM+ and decreases for SAM- perturbations, and is insensitive to model resolution; and
- an initial adjustment of the density-latitude overturning circulation, Ψ_{σ_2}, that is comparable to that of Ψ_w, but subsequently decays in time at a rate that depends on model resolution.

This analysis portrays the process by which the initial overturning response is ingested into the ocean interior; that is, adiabatically along isopycnals, which for the high resolutions simulations with SAM+ perturbations occurs at a rate of order 1° latitude per year.

5 Conclusion

We have presented a novel methodology for perturbing global ocean–sea-ice models driven by prescribed atmospheric forcing. Here, this methodology employs periods of extreme SAM conditions identified in the JRA55-do dataset to branch perturbation simulations from a control. By using periods of extreme yet realistic atmospheric conditions, as opposed to idealised modifications of control conditions, we maintain the physical fidelity of the JRA55-do forcing across its fields. This approach provides confidence that the magnitude of the forcing perturbation is climatologically relevant, even if the timescale of the forcing perturbation is not. The focus here is on extreme SAM conditions, however, this methodology could be used to examine the ocean–sea-ice response to other major climate indices.

The analysis of the perturbation simulations demonstrates the utility of the new methodology for examining the response of the Southern Ocean to extreme SAM forcing conditions. The thermal response to the perturbed forcing, especially the contribution from isopycnal heave, is insensitive to the model resolutions used here; the exception to this is the change of temperature on isopycnals, which intensifies as model resolution is refined, reflecting the important role of eddies in this process. The response of the Southern Ocean overturning circulation to extreme SAM conditions consists of a rapid and sustained adjustment of the wind-driven Deacon cell, and an initial adjustment of the density-latitude overturning circulation that decays in time. The overturning circulation responses are found to project into the interior, propagating northward along isopycnals at a rate of order 1° of latitude per year. It is argued that the adjustment of the overturning in density-latitude coordinates represents the spin-up of the adiabatic eddy field in response to the extreme SAM forcing conditions. Finally, considering the continued strengthening trend of the SAM in the present-day climate, we can anticipate associated increases in the Southern Ocean overturning circulation in depth-latitude coordinates, and an ongoing adjustment of the overturning in density-latitude coordinates and Southern Ocean eddy field.

Acknowledgments

We acknowledge the support of this work from the Earth Systems and Climate Change Hub funded by the Australian Government's National Environmental Science Program (NESP). Many thanks to Navid Constantinou, Ryan Holmes, Qian Li, Adele Morrison and Jan Zika for very helpful discussions, and to the COSIMA consortium (www.cosima.org.au) for making available the ACCESS-OM2 suite of models. We also thank Chris Chapman who proposed the idea of the repeating year extreme SAM perturbation experiments at the Australian Research Council Centre of Excellence for Climate Extremes 2018 SAM workshop. The numerical simulations and analysis were performed with the resources of the National Computational Infrastructure (Canberra, Australia). The ACCESS-OM2 model output is in the process of being uploaded to the COSIMA Model Output Collection; when this process is complete the data will be available from doi:10.4225/41/5a2dc8543105a.

References

Armour, K., Marshall, J., Scott, J., Donohoe, A., & Newsom, E. (2016). Southern Ocean warming delayed by circumpolar upwelling and equatorward transport. *Nature Geoscience*, *9*, 549–554. doi: 10.1038/NGEO2731

Bindoff, N., & McDougall, T. (1994). Diagnosing Climate Change and Ocean Ventilation Using Hydrographic Data. *Journal of Physical Oceanography*, *24*, 1137–1152. doi: 10.1175/1520-0485(1994)024⟨1137:DCCAOV⟩2.0.CO;2

Doddridge, E., Marshall, D., & Hogg, A. (2016). Eddy Cancellation of the Ekman Cell in Subtropical Gyres. *Journal of Physical Oceanography*, *46*, 2995–3010. doi: 10.1175/JPO-D-16-0097.1

Farneti, R., & Delworth, T. (2010). The role of mesoscale eddies in the remote oceanic response to altered Southern Hemisphere winds. *Journal of Physical Oceanography*, *40*, 2348–2354. doi: 10.1175/2010JPO4480.1

Farneti, R., Delworth, T., Rosati, A., Griffies, S., & Zeng, F. (2010). The role of mesoscale eddies in the rectification of the Southern Ocean response to climate change. *Journal of Physical Oceanography*, *40*, 1539–1557. doi: 10.1175/2010JPO4353.1

Farneti, R., Downes, S., Griffies, S., Marsland, S., Behrens, E., Bentsen, M., . . . Yeager, S. (2015). An assessment of Antarctic Circumpolar Current and Southern Ocean meridional overturning circulation during 1958–2007 in a suite of interannual CORE-II simulations. *Ocean Modelling*, *93*, 84–120. doi: 10.1016/j.ocemod.2015.07.009

Frölicher, T., Sarmiento, J., Paynter, D., Dunne, J., Krasting, J., & Winton, M. (2015). Dominance of the Southern Ocean in anthropogenic carbon and heat uptake in CMIP5 models. *Journal of Climate*, *28*, 862–886. doi: 10.1175/JCLI-D-14-00117.1

Gent, P. (2016). Effects of Southern Hemisphere Wind Changes on the Meridional Overturning Circulation in Ocean Models. *Annual Review of Marine Science*, *8*, 79–94. doi: 10.1146/annurev-marine-122414-033929

Gent, P., & Danabasoglu, G. (2011). Response to Increasing Southern Hemisphere Winds in CCSM4. *Journal of Climate*, *24*, 4992–4998. doi: 10.1175/JCLI-D-10-05011.1

Gent, P., & McWilliams, J. (1990). Isopycnal mixing in ocean circulation models. *Journal of Physical Oceanography*, *20*, 150–155. doi: 10.1175/1520-0485(1990)020⟨0150:IMIOCM⟩2.0.CO;2

Gong, D., & Wang, S. (1999). Definition of Antarctic Oscillation Index. *Geophysical Research Letters*, *26*, 459–462. doi: 10.1029/1999GL900003

Griffies, S., Gnanadesikan, A., Dixon, K., Dunne, J., Gerdes, R., Harrison, M., . . . Zhang, R. (2005). Formulation of an ocean model for global climate simulations. *Ocean Science*, *1*, 45–79. doi: 10.5194/os-1-45-2005

Hallberg, R. (2013). Using a resolution function to regulate parameterizations of oceanic mesoscale eddy effects. *Ocean Modelling*, *72*, 92–103. doi: 10.1016/J.OCEMOD.2013.08.007.

Hazel, J., & Stewart, A. (2019). Are the Near-Antarctic Easterly Winds Weakening in Response to Enhancement of the Southern Annular Mode? *Journal of Climate*, *32*, 1895–1918. doi: 10.1175/JCLI-D-18-0402.1

Hofmann, M., & Morales-Maqueda, M. (2011). The response of Southern Ocean eddies to increased midlatitude westerlies: A non-eddy resolving model study. *Geophysical Research Letters*, *38*, L03605. doi: 10.1029/2010GL045972

Kiss, A., Hogg, A., Hannah, N., Dias, F., Brassington, G., Chamberlain, M., . . . Zhang, X. (2020). ACCESS-OM2: A Global Ocean–Sea-Ice Model at Three Resolutions. *Geoscientific Model Development*, *13*, 401–442. doi: 10.5194/gmd-13-401-2020

Kosempa, M., & Chambers, D. (2014). Southern Ocean velocity and geostrophic transport fields estimated by combining Jason altimetry and Argo data. *Journal of Geophysical Research: Oceans*, *119*, 4761–4776. doi: 10.1002/2014JC009853

Li, Q., Lee, S., England, M., & McClean, J. (2019). Seasonal-to-Interannual Response of Southern Ocean Mixed Layer Depth to the Southern Annular Mode from a Global 1/10° Ocean Model. *Journal of Climate*, *32*, 6177–6195. doi: 10.1175/JCLI-D-19-0159.1

Llovel, W., & Terray, L. (2016). Observed Southern Upper-Ocean Warming Over 2005–2014 and Associated Mechanisms. *Environmental Research Letters*, *11*, 124023. doi: 10.1088/1748-9326/11/12/124023

Locarnini, R., Mishonov, A., Antonov, J., Boyer, T., Garcia, H., Baranova, O., . . . Seidov, D. (2013). World Ocean Atlas 2013, Volume 1: Temperature. *NOAA Atlas NESDIS*, *73*.

Lovenduski, N., & Gruber, N. (2005). Impact of the Southern Annular Mode on Southern Ocean circulation and biology. *Geophysical Research Letters*, *32*, L11603. doi: 10.1029/2005GL022727

Marshall, G. (2003). Trends in the Southern Annular Mode from observations and reanalyses. *Journal of Climate*, *16*, 4134–4143. doi: 10.1175/1520-0442(2003)016⟨4134:TITSAM⟩2.0.CO;2

Marshall, J., Scott, J., Armour, K., Campin, J.-M., Kelley, M., & Romanou, A. (2015). The ocean's role in the transient response of climate to abrupt greenhouse gas forcing. *Climate Dynamics*, *44*, 2287–2299. doi: 10.1007/s00382-014-2308-0

Redi, M. (1982). Oceanic Isopycnal Mixing by Coordinate Rotation. *Journal of Physical Oceanography*, *12*, 1154–1158. doi: 10.1175/1520-0485(1982)012⟨1154:OIMBCR⟩2.0.CO;2

Roemmich, D., Church, J., Gilson, J., Monselesan, D., Sutton, P., & Wijffels, S. (2015). Unabated planetary warming and its ocean structure since 2006. *Nature Climate Change*, *5*, 240–245. doi: 10.1038/nclimate2513

Sallèe, J., Speer, K., & Rintoul, S. (2010). Zonally asymmetric response of the Southern Ocean mixed-layer depth to the Southern Annular Mode. *Nature Geoscience*, *3*, 273–279. doi: 10.1038/NGEO812

Sen Gupta, A., & England, M. (2006). Coupled Ocean–Atmosphere–Ice Response to Variations in the Southern Annular Mode. *Journal of Climate*, *19*, 4457–4485. doi: 10.1175/JCLI3843.1

Spence, P., Griffies, S., England, M., Hogg, A., Saenko, O., & Jourdain, N. (2014). Rapid subsurface warming and circulation changes of Antarctic coastal waters by poleward shifting winds. *Geophysical Research Letters*, *41*, 4601–4610. doi: 10.1002/2014GL060613

Stewart, K., Hogg, A., Griffies, S., Heerdegen, A., Ward, M., Spence, P., & England, M. (2017). Vertical resolution of baroclinic modes in global ocean models. *Ocean Modelling*, *113*, 50–65. doi: 10.1016/j.ocemod.2017.03.012

Stewart, K., Kim, W., Urakawa, S., Hogg, A., Yeager, S., Tsujino, H., ... Danabasoglu, G. (2020). JRA55-do-based repeat year forcing datasets for driving ocean–sea-ice models. *Ocean Modelling*, *147*, 101557. doi: 10.1016/j.ocemod.2019.101557

Thompson, D., & Solomon, S. (2002). Interpretation of recent Southern Hemisphere climate change. *Science*, *296*, 895–899. doi: 10.1126/science.1069270

Thompson, D., & Wallace, J. (2000). Annular Modes in the Extratropical Circulation. Part I: Month-to-Month Variability. *Journal of Climate*, *13*, 1000–1016. doi: 10.1175/1520-0442(2000)013⟨1000:AMITEC⟩2.0.CO;2

Thompson, D., Wallace, J., & Hegerl, G. (2000). Annular Modes in the Extratropical Circulation. Part II: Trends. *Journal of Climate*, *13*, 1018–1036. doi: 10.1175/1520-0442(2000)013⟨1018:AMITEC⟩2.0.CO;2

Treguier, A., Sommer, J. L., Molines, J., & Cuevas, B. d. (2010). Response of the Southern Ocean to the Southern Annular Mode: Interannual Variability and Multidecadal Trend. *Journal of Physical Oceanography*, *40*, 1659–1668. doi: 10.1175/2010JPO4364.1

Tsujino, H., Urakawa, S., Nakano, H., Small, R., Kim, W., Yeager, S., ... Yamazaki, D. (2018). JRA-55 based surface dataset for driving ocean–sea-ice models (JRA55-do). *Ocean Modelling*, *130*, 79–139. doi: 10.1016/j.ocemod.2018.07.002

Waugh, D., & Haine, T. (2020). How rapidly do the southern subtropical oceans respond to wind stress changes? *Journal of Geophysical Research: Oceans*. doi: 10.1029/2020JC016236

Waugh, D., Hogg, A., Spence, P., England, M., & Haine, T. (2019). Response of Southern Ocean Ventilation to Changes in Midlatitude Westerly Winds. *Journal of Climate*, *32*, 5345–5361. doi: 10.1175/JCLI-D-19-0039.1

Zheng, F., Li, J., Clark, R., & Nnamchi, H. (2013). Simulation and Projection of the Southern Hemisphere Annular Mode in CMIP5 Models. *Journal of Climate*, *26*, 9860–9879. doi: 10.1175/JCLI-D-13-00204.1

Zika, J., England, M., & Sijp, W. (2012). The Ocean Circulation in Thermohaline Coordinates. *Journal of Physical Oceanography*, *42*, 708–724. doi: 10.1175/JPO-D-11-0139.1

Zweng, M., Reagan, J., Antonov, J., Locarnini, R., Mishonov, A., Boyer, T., ... Biddle, M. (2013). World Ocean Atlas 2013, Volume 2: Salinity. *NOAA Atlas NESDIS*, *74*.

Supporting Information for "Response of the Southern Ocean overturning circulation to extreme Southern Annular Mode conditions"

K.D. Stewart[1,2], A.McC. Hogg[1,3], M.H. England[2,3], and D.W. Waugh[4,5]

[1]Research School of Earth Sciences, Australian National University, Canberra, Australia

[2]Climate Change Research Centre, University of New South Wales, Sydney, Australia

[3]Australian Research Council Centre of Excellence for Climate Extremes

[4]Department of Earth and Planetary Sciences, The Johns Hopkins University, Baltimore, USA

[5]School of Mathematics and Statistics, University of New South Wales, Sydney, Australia

Contents of this file

1. Figures S1 to S3

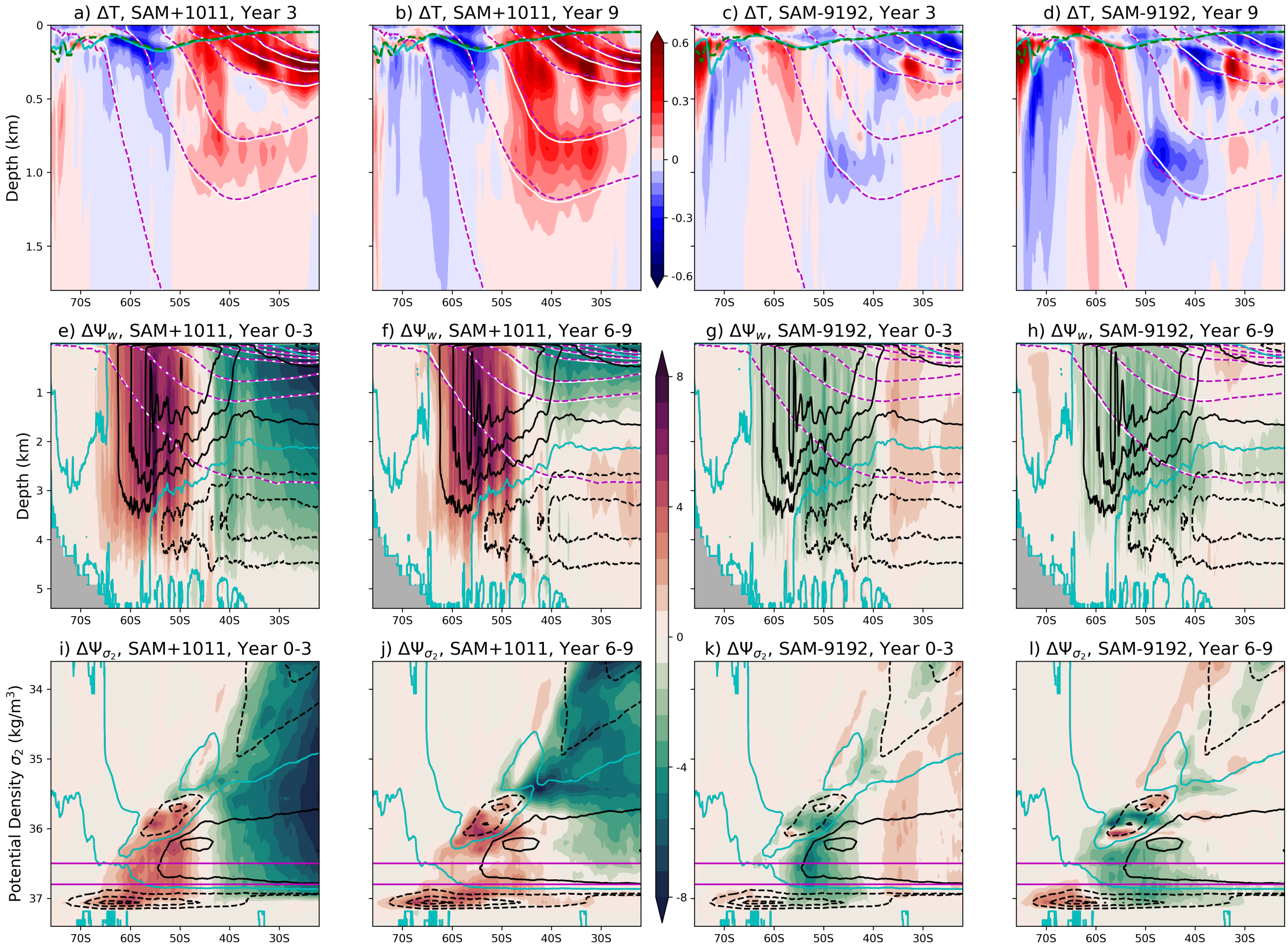

Figure S1. SUPPLEMENTARY FIGURE 1: Equivalent to Figure 2. a-d) Distributions of the Year 3 (a,c) & 9 (b,d) temperature anomalies from the 0.1° ACCESS-OM2-01 for (a,b) SAM+1011 and (c,d) SAM-9192 simulations. The white and dashed magenta contours represent the SAMx and RYF9091 isopycnals at $\sigma_2 = 0.5\,\mathrm{kg/m^3}$ intervals, respectively, spanning $\sigma_2 = 34$–$37\,\mathrm{kg/m^3}$ inclusive, with the cyan and dashed green contours representing the respective mixed-layer depths. e-h) The w-streamfunction anomalies of the ACCESS-OM2-01 simulations with SAM+1011 (e,f) and SAM-9192 (g,h) averaged for the years 0-3 (e,g) and 6-9 (f,h). Contoured in black is the Ψ_w for the RYF9091 case at $\pm 7.5\,\mathrm{Sv}$ intervals with the $0\,\mathrm{Sv}$ contour in cyan. The white and dashed magenta contours represent the same isopycnals as in (a-d). Panels (i-l) depict a similar analysis to panels (e-h) but for the σ_2-streamfunction anomalies. The magenta lines in (i-l) at 36.5 and $36.8\,\mathrm{kg/m^3}$ indicate the regions of interest for Figure 3.

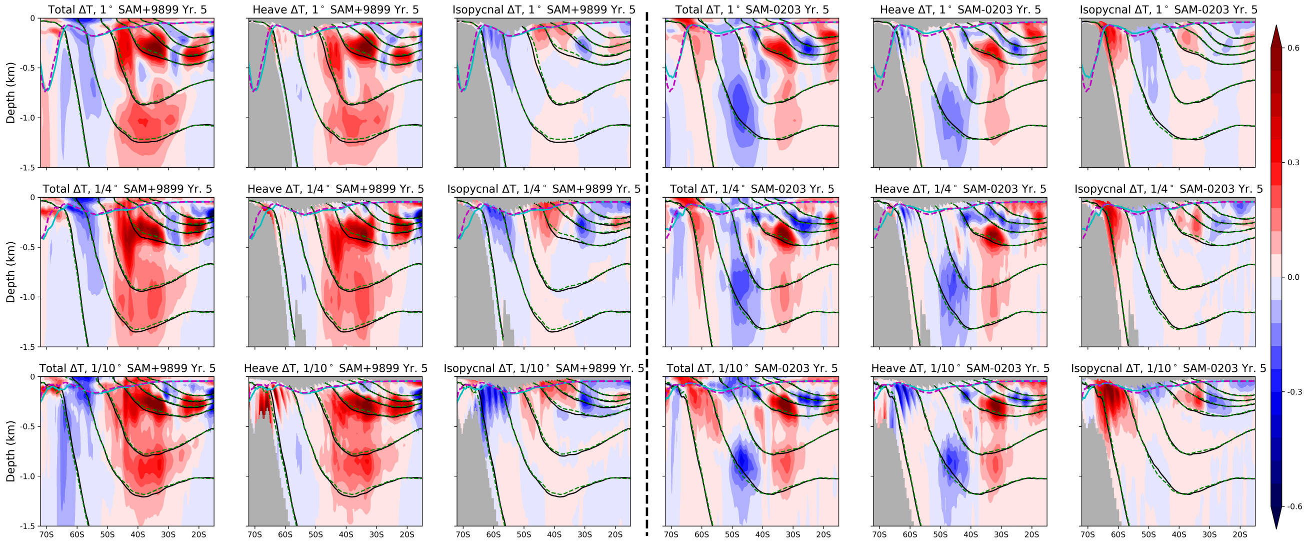

Figure S2. SUPPLEMENTARY FIGURE 2. Distributions of the Year 5 temperature anomalies for the SAM+9899 (cols. 1-3) and SAM-0203 (cols. 4-6) cases at 1°, 0.25° and 0.1° resolutions (rows 1-3, respectively). Columns 1 & 4 show the total temperature anomalies; columns 2 & 5 show the temperature anomaly associated with heave; and columns 3 & 6 show the temperature anomaly due temperature changes on isopycnals. The black and dashed green contours represent the SAMx and RYF9091 isopycnals at $\sigma_2 = 0.5\,\mathrm{kg/m^3}$ intervals, respectively, spanning $\sigma_2 = 34$–$37\,\mathrm{kg/m^3}$ inclusive, with the cyan and dashed magenta contours representing the respective mixed-layer depths. The temperature anomaly due to heave is calculated by remapping the zonally-averaged temperature in latitude-σ_2 space of the RYF9091 case back into latitude-depth space using the σ_2-depth relationship of a given SAMx case. The temperature anomaly due to the change of temperature on isopycnals is calculated by remapping the zonally-averaged temperature differences between the SAMx and RYF9091 in latitude-σ_2 space back into latitude-depth space using the σ_2-depth relationship of RYF9091. The greyed regions here are an artefact of transformation between depth and σ_2 spaces.

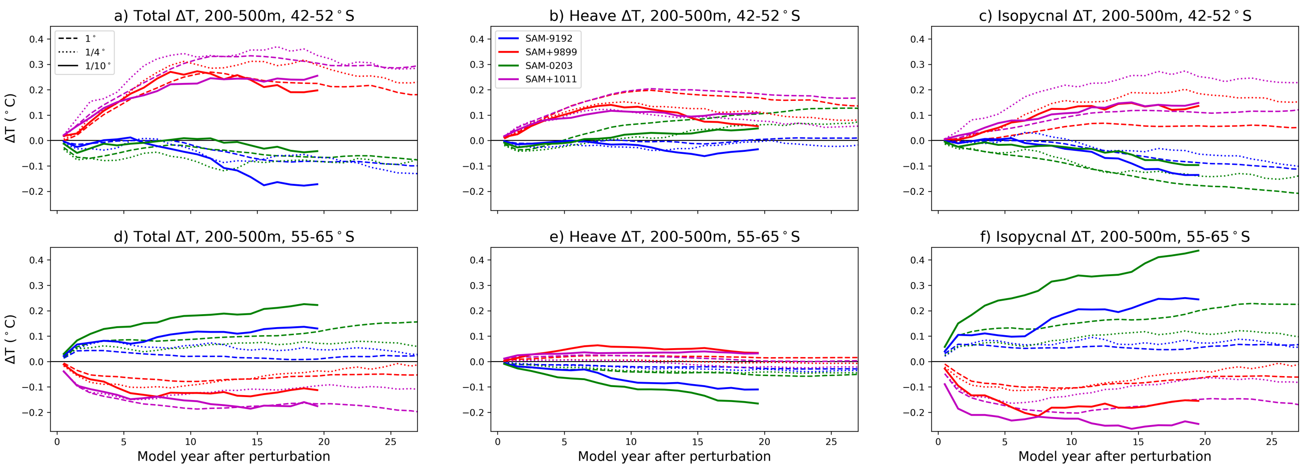

Figure S3. SUPPLEMENTARY FIGURE 3. Timeseries of the extended responses in regions north (a-c) and south (d-f) of the wind speed maximum for the total (a,d), heave (b,e) and isopycnal (c,f) temperature anomalies.